Title: Electrically-Driven Proton Transfer Promotes Brønsted Acid Catalysis by Orders of Magnitude

Authors: Karl S. Westendorff[1], Max J. Hülsey[2], Thejas S. Wesley[1], Yuriy Román-Leshkov[1,2*], Yogesh Surendranath[1,2*]

Affiliations:

[1]Department of Chemical Engineering, Massachusetts Institute of Technology; Cambridge, Massachusetts 02139, United States

[2]Department of Chemistry, Massachusetts Institute of Technology; Cambridge, Massachusetts 02139, United States

*Corresponding author. Email: yroman@mit.edu, yogi@mit.edu

Abstract:

Electric fields play a key role in enzymatic catalysis and can enhance reaction rates by 100,000-fold, but the same rate enhancements have yet to be achieved in thermochemical heterogeneous catalysis. Herein, we probe the influence of catalyst potential and interfacial electric fields on heterogeneous Brønsted acid catalysis. We observe that variations in applied potential of ~360 mV lead to a ~100,000-fold rate enhancement for 1-methylcyclopentanol dehydration catalyzed by carbon-supported phosphotungstic acid. Mechanistic studies support a model in which the interfacial electrostatic potential drop drives quasi-equilibrated proton transfer to the adsorbed substrate prior to rate-limiting C-O bond cleavage. Large increases in rate with potential are also observed for the same reaction catalyzed by Ti/TiO_yH_x and for the Friedel Crafts acylation of anisole with acetic anhydride by carbon-supported phosphotungstic acid. This work highlights the important role interfacial electrochemical potential can play in Brønsted acid catalysis.

One-Sentence Summary:

Varying the surface electrochemical potential promotes the rate of Brønsted acid catalysis by up to 100,000-fold.

Main Text:

Electrically-Driven Proton Transfer Promotes Brønsted Acid Catalysis by Orders of Magnitude

Nature generates strong, oriented electric fields in enzymes by precisely placing charged amino acid residues around substrate binding pockets to promote biological catalysis (*1–3*). Similarly, when electrode surfaces are electrically charged, the accumulation of opposing ionic charge in solution generates a sharp electrostatic potential gradient and a correspondingly large oriented electric field at the metal/solution interface (*4*). For electrochemical half-reactions which involve the net transfer of electrons to or from the electrode, the change in free energy and corresponding rate of the half-reaction is known to be strongly dependent on the electrode potential. Thus, small changes (on the order of 100s of mV) in surface electrochemical potential lead to orders of magnitude enhancements in reaction rate (**Fig. 1a**) (*5–11*). This contrasts with redox neutral thermochemical reactions, where there is no net exchange of electrons to or from the catalytic interface and therefore no change in the reaction's free energy upon varying surface potential. Consequently, attempts to utilize surface potentials to promote thermochemical transformations generally scale weakly with potential, and the mechanisms underlying these relatively modest promotional effects remain unclear (**Fig. 1b**) (*12–17*).

For many electrochemical half-reactions, varying the applied potential acts to augment the half-reaction rate by driving rate-controlling elementary proton-coupled electron transfer (PCET) steps in the reaction sequence (*18–20*). We therefore posited that if an elementary PCET step were embedded within an overall thermochemical reaction, the strong potential-dependence of the PCET step could be leveraged to promote non-Faradaic thermochemical catalysis. Since interfacial PCET (I-PCET) reactions involve proton exchange across the electric double layer, the foregoing logic suggests that thermochemical reactions catalyzed by proton transfer, namely those subject to Brønsted acid catalysis (BAC), could be dramatically promoted via the polarization dependence of rate-controlling elementary I-PCET steps (**Fig. 1c**). Importantly, this promotion strategy does not require additional energy input into the system beyond polarizing the catalytic interface, exposing a highly energy-efficient approach for accelerating redox-neutral thermochemical reactions.

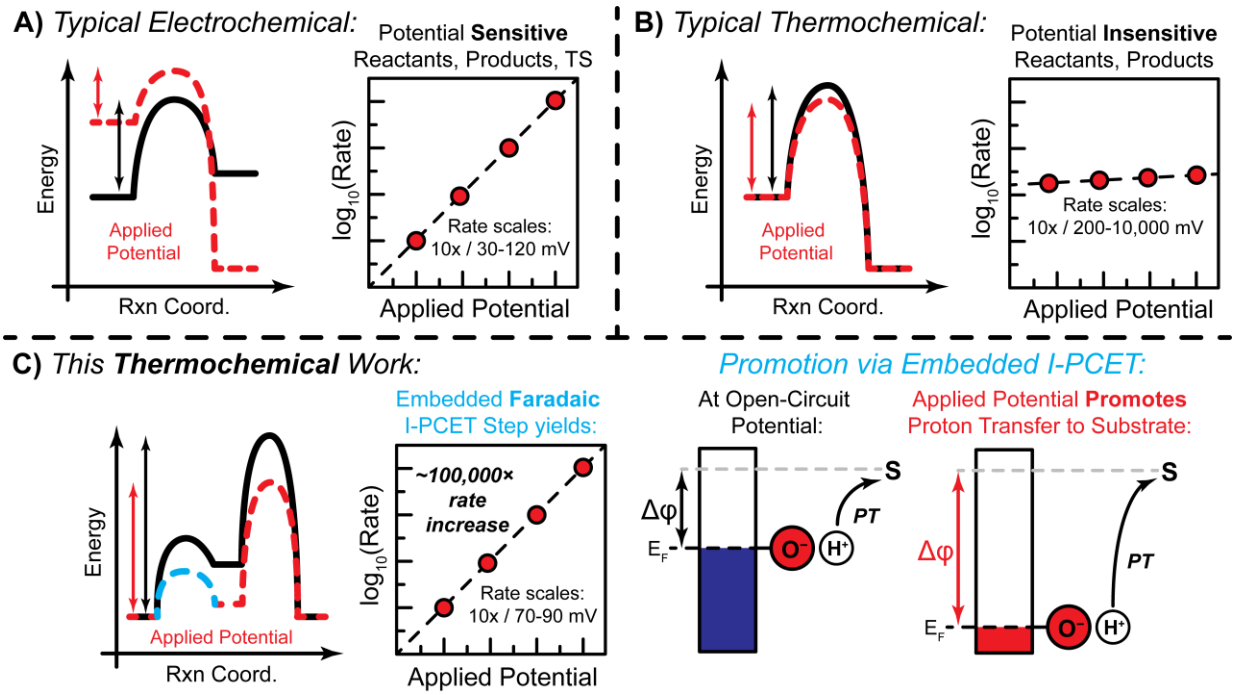

Fig. 1. Similarities and contrasts between typical electrochemical and thermochemical reactions, and this work. (**A**) For electrochemical reactions, varying the applied potential alters the overall free energy change for the reaction (left) and can induce large changes in reaction rate (right). (**B**) For thermochemical reactions, varying potential does not change the free energy of reaction (left) and most thermochemical reactions have modest dependence on rate (right). (**C**). We show that polarization can dramatically impact the rate of a thermochemical reaction sequence with an embedded interfacial PCET step (left). The electrostatic potential drop at the surface drives protons to the substrate upon positive polarization, and this driving force increases with applied oxidative potential (right).

In this work, we examined the potential-dependence of BAC. For a model dehydration reaction of 1-methylcyclopentanol with carbon-supported phosphotungstic acid (PTA), we find that interfacial polarization can alter BAC turnover frequencies (TOFs) by as much as 5 orders of magnitude, with potential-dependent scale factors similar to those of electrochemical transformations (10× per ~100 mV) despite no change in the net reaction free energy. Mechanistic studies suggest that the strong potential dependence arises from an electrically-driven shift in the reaction quotient for a pre-RDS equilibrium proton exchange step between PTA and 1-methylcyclopentanol which precedes rate-determining C-O bond cleavage. Varying the potential serves to alter the catalyst's effective acidity, resulting in an accumulation of protonated alcohol species reacting in the rate-limiting step, thereby enhancing the reaction rate. We further find that polarization promotes BAC by oxide-coated titanium electrodes and for a Friedel-Crafts acylation reaction, evincing the generality of this promotion mechanism. These findings emphasize the powerful role that interfacial polarization can play in thermochemical catalysis.

Brønsted Acid Catalytic Activity is Strongly Dependent on Interfacial Potential

To investigate the effect of electrochemical potential on BAC catalysis, we examined the dehydration of 1-methylcyclopentanol in acetonitrile (MeCN) catalyzed by phosphotungstic acid (PTA) supported on Vulcan carbon (PTA/C). Tetrabutylammonium hexafluorophosphate ([TBA][PF_6]) served as the supporting electrolyte. This probe system was selected specifically to

circumvent any convolution from Faradaic reactions, as the W^{VI} centers in PTA are immune to oxidation, the MeCN solvent has a large electrochemical window, and tertiary alcohols are resistant to oxidation at the potentials used in this study (*21–23*). We initially focused on an alcohol dehydration because of its relatively simple mechanism compared to other BAC reactions. In this system, all reactions were run at 40°C in a solution of a 0.1 M 1-methylcyclopentanol with 0.1 M [TBA][PF_6] as electrolyte and 0.1 M tri-*tert*-butylbenzene as internal standard. We report all rates vs. the decamethylferrocene redox couple ($DmFc/DmFc^+$) in this solution unless otherwise stated.

We conducted initial experiments in a batch reactor using a colloidal suspension of PTA/C and measured reaction rates by product formation as quantified by NMR spectroscopy of reaction aliquots. Since every active site in a PTA/C colloidal suspension cannot be wired to an external circuit, we conducted our initial studies by "wirelessly" polarizing the catalyst using redox buffers in solution.

In this polarization method, the reduced and oxidized components of a redox buffer in solution add and remove electrons from the conductive colloidal carbon particles, respectively, to establish electrochemical equilibrium at the carbon/solution interface. This equilibrium sets the electrochemical potential of the carbon particles in a Nernstian fashion based on the standard reduction potential of the redox species and the ratio of its reduced and oxidized components. We previously demonstrated the efficacy of this polarization method and employ it here to set the potential of the PTA/C catalyst suspension (*24*).

We chose [$Fe(phen)_3$][PF_6]$_2$ and [$Fe(phen)_3$][PF_6]$_3$ and their hexamethylated derivatives [$Fe(5,6\text{-}Me_2\text{-}phen)_3$][$PF_6$]$_2$ / [$Fe(5,6\text{-}Me_2\text{-}phen)_3$][$PF_6$]$_3$ as redox buffers because of their fast outer-sphere electron transfer rates and because these organometallic complexes are coordinatively saturated, thereby inhibiting covalent binding interactions with the catalytic surface. Indeed, we found that these redox buffers have negligible catalytic activity on their own and that varying the overall concentration of the redox buffer does not significantly influence the rate (**Figs. S12** and **S13**) of the BAC reaction.

We find that BAC of 1-methylcyclopentanol dehydration at 40°C is strongly dependent on potential in these spontaneous polarization studies. Using a 1:1 [$Fe(5,6\text{-}Me_2\text{-}phen)_3$][$PF_6$]$_2$ / [$Fe(5,6\text{-}Me_2\text{-}phen)_3$][$PF_6$]$_3$ buffer to set the potential of the catalyst to 1170 mV, we measured a TOF of 0.029 s^{-1}. We increased the potential of the catalyst up to 1260 mV with a 1:5 [$Fe(phen)_3$][PF_6]$_2$ / [$Fe(phen)_3$][PF_6]$_3$ redox buffer and measured a TOF of 0.84 s^{-1}, evincing a ~30 fold increase in TOF upon increasing the pinned potential by 90 mV (**Fig. 2**, blue points). We find that unmodified carbon powder is responsible for <10% of the observed rate when polarized.

To further extend the potential range and explore the extent of the promotion effect, we examined BAC catalysis with PTA deposited on Sigracet 39 BB carbon paper electrodes. These modified carbon electrodes served as the working electrodes in a conventional undivided three-electrode electrochemical cells, allowing for direct polarization of the interface via a potentiostat (**Fig. S14**). We measured rates by product formation via NMR spectroscopy of reaction aliquots under the same reaction conditions as employed in the wireless polarization experiments. At an applied potential of 1390 mV, we measured a TOF of 41 s^{-1} which increased to 2860 s^{-1} at an applied potential of 1530 mV (**Fig. 2**, red points). The background reactivity of the carbon support was subtracted from the raw rates to produce these TOF values (**Fig. S16**). The TOF vs. potential data for both the wired and wireless experiments fall on a common trendline with the TOF increasing by approximately five orders of magnitude over a potential range of 360 mV (**Fig. 2**). The common trendline displays a slope corresponding to a ten-fold increase in rate per 76 mV increase in catalyst

potential. Immobilization of PTA on carbon is known to attenuate BAC rates relative to that of homogeneous PTA (*25*) (**Fig. 2**, orange dotted line), yet electrical polarization exposes BAC rates that exceed that of homogeneous PTA by several orders of magnitude. These data indicate that Brønsted acid catalyzed alcohol dehydration by PTA/C is strongly dependent on the electrochemical potential of the catalyst.

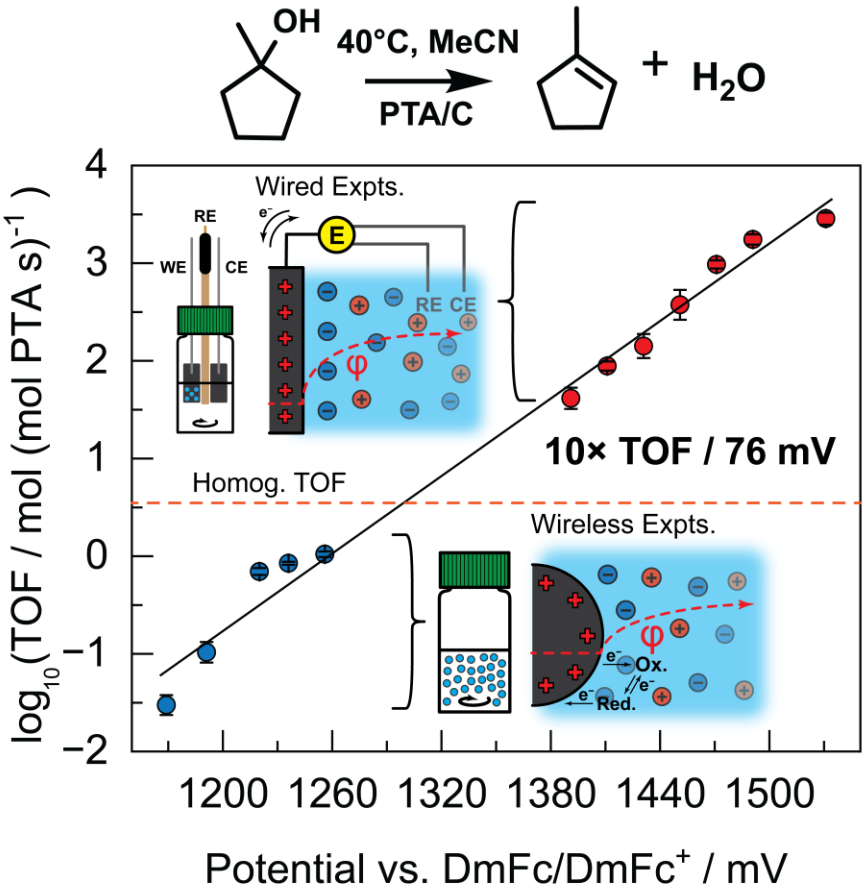

Fig. 2. Turnover frequency (TOF) dependence on applied electrochemical potential for PTA/C catalyzed dehydration of 1-methylcyclopentanol. Potential dependence of the TOF of colloidal 5% PTA/C polarized by exposure to varying molecular redox buffers (blue data points). Potential dependence of TOF for PTA/C electrodes polarized potentiostatically (red data points). TOF for unpolarized homogeneous PTA (orange dotted line). All reactions were run at 40°C in a solution of a 0.1 M 1-methylcyclopentanol in MeCN with 0.1 M [TBA][PF_6] as electrolyte and 0.1 M tri-*tert*-butylbenzene as internal standard. Reaction conditions are further detailed in **Supplementary Sections 3.5** and **4.3**.

To elucidate the origin of this dramatic promotion in reaction rate, we carried out a series of control experiments. For both the wireless and wired experiments, rate data were collected under conditions of differential conversion and the rate of product formation was found to be constant over time (**Figs. S17** and **S18**). This finding precludes convolution from reaching equilibrium conversion and likely precludes substantial active site deactivation or active site generation over the course of our measurements. To assess whether the applied potential altered the bulk reaction medium, we examined the homogeneous catalytic activity after the reaction by retaking NMR measurements of reaction aliquots after the PTA/C catalyst was removed from the reaction

medium. We observed no significant changes in product yield over time upon removing the PTA/C, suggesting that neither catalyst leaching nor the generation of a soluble protic species is responsible for the observed scaling of reaction rate with potential (**Figs. S19** and **S20**). This finding is also consistent with the observed linear reaction profiles. To examine whether Faradaic pathways significantly contribute to the observed trend in reactivity with potential, we calculated ratios of the measured molar rates of product formation over the steady-state currents for the wired polarization experiments. At 1390 mV, this ratio is over 1100, and at 1530 mV vs. $DmFc/DmFc^+$ this ratio is over 430. Similar ratios were found at intermediate potentials with no clear trend, suggesting that parasitic Faradaic reactions are not responsible for the observed promotion in BAC (**Fig. S21**). To determine whether the observed promotion effect could be ascribed to a permanent change in catalyst structure, we examined the reversibility of the promotion effect by modulating the potential of the working electrode in a single experiment. Switching from 1530 mV to 1390 mV led to an immediate drop in TOF from 1230 s^{-1} to 8 s^{-1}, and a TOF of 1230 s^{-1} was immediately recovered upon switching back to 1530 mV (**Fig. S22**). These findings suggest that the observed change in catalytic rate cannot be attributed to an irreversible change in the catalyst or support structure. We additionally measured the reaction order with respect to 1-methylcyclopentanol to test whether transport artifacts could convolute the measured rates. We found that the reaction rate is 0^{th} order in reactant concentration, indicating that transport artifacts do not substantially convolute our rate measurements (**Fig. S23**, see **Supplementary Section 5.8** for detailed discussion).

Next, we conducted a set of experiments to better understand the dehydration reaction mechanism. To examine whether C-O bond cleavage is reversible, we conducted an ^{18}O isotope tracing experiment by injecting $H_2{}^{18}O$ into the reaction solution and analyzing ^{18}O incorporation in the reactant after measurable conversion (**Fig. S25**). We found no detectable ^{18}O incorporation into 1-methylcyclopentanol via GC-MS after running the reaction to a conversion comparable to that in our kinetic studies, suggesting that C-O bond cleavage is irreversible in this system (**Fig. S26**) (*26*).

To probe the effect of the interfacial potential drop and corresponding field strength on the reaction, we varied the electrolyte concentration and measured the reaction rate scaling with potential. Whereas, we observed a 10× rate enhancement for every 70 mV change in potential in a 0.1 M $[TBA][PF_6]$ electrolyte, the scaling attenuates to 10× every 120 mV in 0.05 M electrolyte, and we observe no significant scaling with potential in 0.005 M electrolyte (**Fig. S27**). This trend suggests the potential-driven kinetic enhancements are sensitive to the gradient in electrostatic potential profile in the double layer rather than solely the absolute value of the potential at the surface (*4*, *27*). We note substitution of $[TBA][PF_6]$ with [TBA][TFSI] returns the same reaction rate at the highest potential sampled, suggesting that the electrolyte is not directly participating in the reaction other than establishing the double layer potential profile.

The preceding control experiments and mechanistic studies provide the basis for a mechanistic model for potential-dependent BAC depicted in **Fig. 3a**. Due to the 0^{th} order dependence on 1-methylcyclopentanol concentration, we infer that the active sites are fully saturated with adsorbed alcohol (*28*), making the surface bound alcohol the most abundant surface species. Alcohol adsorption is followed by a putative potential-dependent proton transfer step (an I-PCET reaction) from a W-OH moiety to the adsorbed 1-methylcyclopentanol. We then invoke rate-limiting C-O bond cleavage to release water and generate a tertiary carbocation, which rapidly transfers a proton to the PTA/C active sites, regenerating the catalyst and furnishing the olefin product upon desorption. The rate-limiting C-O cleavage step is supported by the lack of ^{18}O scrambling in the

system and agrees with previous literature that found E_1 mechanisms dominate at solid-liquid interfaces for tertiary alcohols (*29*, *30*).

In this proposed mechanism, the potential-dependence of the dehydration rate arises from shifting the position of the quasi-equilibrated I-PCET step ($K_2(E)$ in **Fig. 3**) towards product, thereby increasing the population of the pre-RDS oxonium intermediate and lowering the apparent activation free energy of the reaction (**Fig. 3b**). To derive the rate scaling, we apply the following assumptions: (a) the I-PCET step to form the oxonium intermediate resides in minor-equilibrium across the full potential range explored; (b) proton binding to the PTA can be described by a Langmuirian isotherm; (c) the proton traverses the full electrostatic potential drop at the interface in this I-PCET step. With these assumptions, the quasi-equilibrium surface population of the oxonium intermediate will increase by one decade for every 62 mV increase in applied potential under the reaction conditions (at 40°C), and the scale factor for this I-PCET elementary step is expected to translate fully into the scaling of TOF with potential for the overall reaction (see **Supplementary Section 6** for full rate law, potential-dependence derivation, and discussion of potential drop length scale) (*31*–*35*). This predicted scale factor is in close agreement with observed 76 mV/decade scale factor (**Fig. 2**). The effect of electrolyte concentration on potential-rate scaling further supports this model. At high electrolyte concentrations (0.1 M), the electrostatic potential drop is sufficiently steep that we invoke that the adsorbed alcohol experiences a local electrostatic potential comparable to that of bulk solution. Thus, the proton traverses the majority of the interfacial potential drop in the I-PCET step leading to high potential-rate scaling. In contrast, at low electrolyte concentrations (0.005 M [TBA][PF_6]), the electrostatic potential gradient at the interface is shallower, but the length scale for proton transfer from PTA to the adsorbed substrate remains largely unchanged. Consequently, the proton traverses a smaller fraction of the overall potential drop at reduced electrolyte strengths, leading to dramatic attenuation of the potential-rate scaling (**Fig. S28**). Altogether, these data are consistent with a picture of the polarized catalytic interface depicted in **Fig. 3c**.

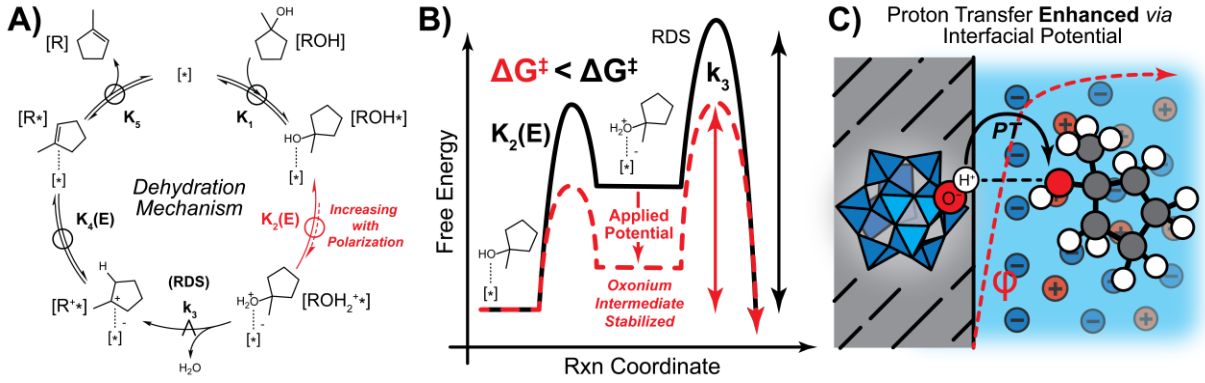

Fig. 3. Schematics of the overall dehydration catalytic cycle, the pre-RDS free energy landscape of the dehydration reaction, and an illustration of the polarized catalytic interface. (**A**) Putative catalytic cycle for PTA/C-catalyzed dehydration of 1-methylcyclopentanol. The key potential-dependent I-PCET step is highlighted in red. (**B**) Free energy landscape diagram of the dehydration reaction (black), illustrating the effect of shifting the pre-RDS equilibrium on the apparent activation free energy of the reaction with applied potential (red). (**C**) Cartoon of the polarized carbon interface with PTA sites donating protons to the substrate. The presence of an interfacial potential drop drives proton transfer, and the proton is invoked to traverse the majority potential drop to recover the experimentally measured rate scaling with potential.

We note that since the dehydration reaction does not involve electron exchange in net (i.e. it is not an electrochemical half-reaction), varying the applied potential cannot alter the overall free energy change for dehydration. Consequently, any effect of the applied potential on the forward I-PCET step (K_2(E), **Fig. 3a**) must be balanced by an opposing effect on the reverse I-PCET step (K_4(E), **Fig. 3a**) that regenerates the catalyst. Thus, in this model, catalyst regeneration via I-PCET from the carbocation to the PTA is expected to be inhibited by 10× for every 62 mV increase in applied potential (at 40°C). However, since this reverse I-PCET is after the RDS, its inhibition with increasing applied potential does not substantially influence the observed kinetics, leading to the observed monotonic increase in reaction rate with positive polarization.

Potential-Dependent BAC Extends to Ti/TiO_yH_x interfaces.

The mechanistic model depicted in **Fig. 3** implies that polarized-induced promotion of BAC should not be limited to a specific material. Indeed, any polarizable interface with surface -OH_x groups should, in principle, be able to function as tunable BACs that respond to interfacial polarization.

To examine this hypothesis, we investigated the same dehydration reaction with polarized Ti foils as working electrodes in a single cell, three-electrode setup connected to a potentiostat. Due to rapid reaction with O_2, Ti foils invariably contain passivating layers of TiO_2 under reaction conditions (*36*). We envisioned that TiO_yH_x defects in this passivating layer could serve as potential-dependent hosts for BAC catalysis. Assuming all surface-exposed Ti(IV) ions on a Ti foil electrode host active sites, we observe a lower-bound TOF for 1-methylcyclopentanol dehydration of 0.03 s^{-1} at 1810 mV. This TOF rises to 0.49 s^{-1} at 1930 mV, evincing a 16× increase in TOF upon increasing the applied potential by 120 mV (**Fig. 4a**). This corresponds to a decade change in TOF for every 87 mV of applied potential.

We next conducted a series of control experiments, analogous to those for the PTA/C system, to better understand the promotion mechanism for the Ti/TiO_yH_x catalyst. Rate data were collected under conditions of differential conversion, and reaction profiles were again linear over the course of the reaction (**Fig. S31**). This suggests that substantial active site deactivation, active site generation, or approaching equilibrium conversion likely do not significantly contribute to our kinetic measurements. We again found no significant changes in product concentration over time for a given aliquot of reaction solution, suggesting that neither catalyst leaching nor the generation of other soluble protic species contributes to our measured kinetics (**Fig. S32**). We then calculated ratios of measured molar rates over steady-state currents for this system. At 1810 mV, this ratio was over 1350, and at 1930 mV this ratio was over 5000. Intermediate potentials had ratios of similar values, indicating that parasitic Faradaic reaction contribute negligibly to the observed reactivity, just as for the PTA/C catalyst (**Fig. S33**).

We again examined whether the promotion effect could be ascribed to irreversible catalyst structural changes by modulating the potential back and forth in a single experiment. Switching from 1930 mV to 1810 mV led to an immediate drop in the lower-bound TOF from 0.33 s^{-1} to 0.003 s^{-1}, and a lower-bound TOF of 0.12 s^{-1} was immediately recovered upon switching back to 1900 mV (**Fig. S34**). Substrate concentration order studies on this system yield the same 0^{th} order dependence on alcohol concentration as in the PTA/C catalyst, indicating that active sites are saturated with reactant and that transport artifacts do not contribute to the observed kinetics (**Fig. S35**). We further examined for the presence of transport artifacts via rotating cylinder electrode experiments and measured the catalyst TOF as a function of rotation speed. We found the TOF to be independent of rotation speed, indicating that transport artifacts do not contribute substantially to the observed kinetics (**Fig. S39**). This corroborates the zero-order dependence on reactant

concentration for this system. Together, these findings suggest a similar mechanistic model for this Ti/TiO_yH_x catalyst as for the PTA/C catalyst.

Since the measured rate-potential scale factor of 87 mV/decade is similar to the 76 mV/decade scaling observed for the PTA/C catalyst, we invoke an analogous picture of the polarized catalytic interface (**Fig. 4b**). Notably, the above mechanism predicts that the reaction rate will become independent of applied potential at sufficiently high potentials that drive the I-PCET step to major equilibrium (K_2(E) in **Fig. 3b** >1). Under these conditions the oxonium intermediate becomes the most abundant surface species and the rate of the reaction is governed purely by the potential-independent rate of C-O bond cleavage (**Fig. S40**). This translates to a potential-independent plateau in the TOF. This plateau region was inaccessible for PTA/C due to substantial parasitic background current beyond 1530 mV, but is observed for the more inert Ti/TiO_yH_x at potentials beyond 1960 mV, with the TOF remaining at ~0.76 s^{-1}, invariant with potential up to 2310 mV (**Fig. S41**). We note explicitly that the reaction is still 0^{th} order in substrate in this potential-independent regime, and so the observed potential-independence does not arise from transport artifacts. Together, this observation of a potential-independent regime further supports the pre-equilibrium I-PCET mechanistic model put forward in **Fig. 2**.

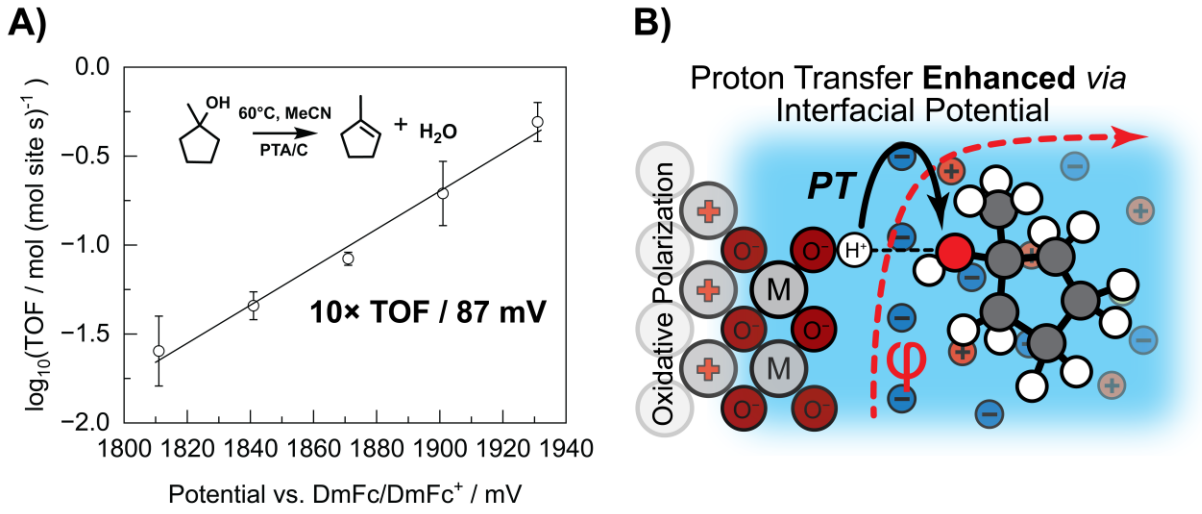

Fig. 4. Potential-dependence of Ti-foil catalyzed dehydration of 1-methylcyclopentanol and a cartoon of the polarized interface. (**A**) Lower-bound TOFs for Ti-foil catalyzed 1-methylcyclopentanol dehydration as function of applied potential. Lower-bound TOFs values were calculated assuming that all surface-exposed Ti atoms host active sites. (**B**) Cartoon depicting polarization-driven proton transfer to the substrate from -OH defects on the passivating TiO_yH_x surface layer. All reactions were run at 60°C in a solution of a 0.1 M 1-methylcyclopentanol in MeCN with 0.1 M [TBA][PF_6] as electrolyte and 0.1 M tri-*tert*-butylbenzene as internal standard. Reaction conditions are further detailed in **Supplementary Section 7.1**.

It is notable that comparable TOFs of the PTA/C and Ti/TiO_yH_x electrodes are achieved at substantially different potentials. While the lower-bound TOFs for the Ti/TiO_yH_x system may be gross underestimates, this factor alone is insufficient to explain the 630 mV potential offset in TOFs between the two catalysts. We speculate that differences in the onset potential of reactivity stem at least partially from the innate acidity of these materials. As TiO_yH_x is an intrinsically weaker acid than PTA, the former requires a greater applied potential to lower its effect pKa to a level sufficient to turn on Brønsted acid catalysis at measureable rates (*37*, *38*). We further

speculate that the slightly higher scale factor, 87 vs. 76 mV/decade, may arise from a small potential drop through the dielectric titanium oxide layer that separates the metallic Ti from the surface-exposed TiO_yH_x active sites (*39*). Overall, these data point to the generality of the observed BAC promotion effect via interfacial electrical polarization and suggest that a wide variety of catalysts may be promoted via this methodology.

The Promotion Effect Extends to Brønsted Acid Catalyzed Acylation

To explore the generality of interfacial electric field promotion, we examined a completely different BAC reaction class, a Friedel Crafts acylation, which results in net C-C bond formation rather than dehydration. Specifically, we investigated the acylation of anisole with acetic anhydride to produce para-methoxyacetophenone and acetic acid. Akin to the dehydration reaction system described previously, the overall reaction cannot reasonably be broken down into Faradaic half-reactions.

We conducted wired polarization experiments, analogous to those for the 1-methylcyclopentanol dehydration reaction, for this acylation reaction. We again used PTA dropcast onto carbon paper as a working electrode and varied its potential in the same cell configuration as the dehydration systems. We again measured the rate of product formation via NMR spectroscopy of reaction aliquots (**Figs. S42** and **S43**). The reaction was run at 70°C in a solution of a 9:1 molar ratio of anisole:acetic anhydride with 1.2 M [TBA][PF_6] as electrolyte.

As for the dehydration reaction, we find that acylation is also strongly potential dependent. The TOF for PTA/C catalyzed acylation increases from 0.66 s^{-1} at 1250 mV vs. Ag/AgCl to 11120 s^{-1} at 1295 mV (**Fig. 5**). We observed no background activity from the carbon paper support. The TOF vs. potential data produce a trendline where the TOF increases approximately four orders of magnitude over a potential range of 45 mV, thereby representing a scale factor of a 10-fold change in TOF for every ~13 mV of applied potential.

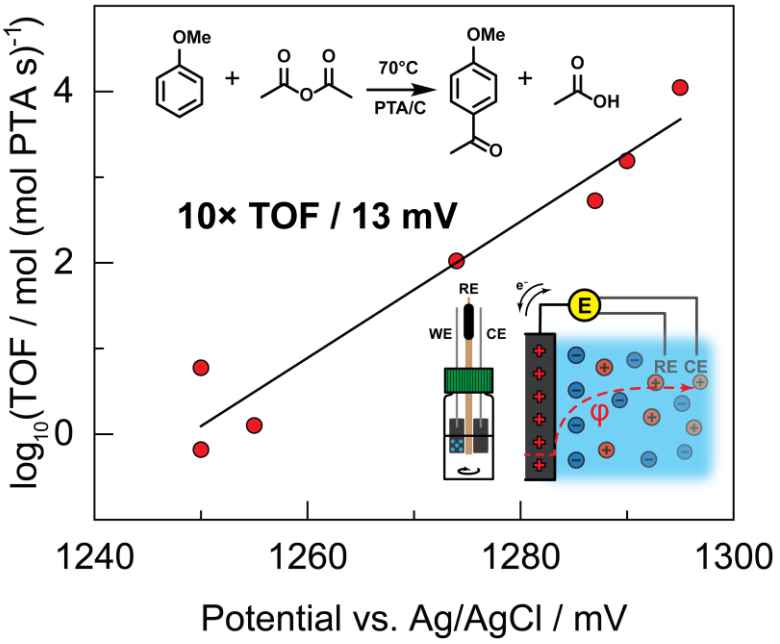

Fig. 5. Potential-dependence of PTA/C catalyzed acylation of anisole. TOF for PTA/C catalyzed acylation of anisole with acetic anhydride as a function of applied potential. All reactions were run at 70°C in a solution of a 0.84 M acetic anhydride in anisole with 1.2 M [TBA][PF_6] as

electrolyte and internal standard. Reaction conditions are further detailed in **Supplementary Section 8.1**.

We performed control experiments analogous to those for the PTA/C and Ti/TiO_yH_x dehydration systems to better understand the potential dependence observed here. To minimize contributions from changes in reaction concentrations, we collected rate data at differential conversion. As for the dehydration reactions, we again observed reaction profiles that are linear over the course of the reaction suggesting that changes in active site identity, quantity, or activity are likely negligible in our system over the timescale of the reaction (**Fig. S44**). To quantify any contributions to catalysis from the reaction solution, we measured the concentration of products over time in a reaction aliquot which is no longer in contact with the polarized interface (**Fig. S45**). We found no significant change in the amount of product over time, suggesting that catalysis is confined entirely to the electrode interface. To determine whether the observed potential dependence was Faradaic in nature, we calculated ratios of molar rates to the steady state current. At the lower potentials tested (~1250 mV vs. Ag/AgCl) these ratios are 0.05-0.2, but they quickly rise to over 2.5 at 1275 mV and to 8.5 at 1295 mV vs. Ag/AgCl (**Fig. S46**). This more complex medium contains species known to undergo oxidative decomposition via, for example, Kolbe oxidation of acetic acid, contributing to much higher parasitic Faradaic currents. Irrespective of the source of the parasitic Faradaic current, the large changes in the above ratios across the potential range suggest that Faradaic processes are not the cause of the observed promotion. We ascribe the large changes in these ratios to the much stronger potential dependence of the BAC promotion relative to parasitic background Faradaic processes.

This finding suggests that potential-dependent Bronsted acid catalysis can be applied across a variety of reactions. While the scale factor of 13 mV per decade in rate is extremely steep and measured over a small potential window, this observation nonetheless emphasizes the importance of measuring and controlling catalyst potential in BAC. While a detailed mechanistic model for this potential-dependent is not yet in hand, we speculate that the dramatic potential dependence may arise from a combination of multiple rate-controlling I-PCET steps and/or cooperative non-Langmuirian adsorption isotherms in this exotic reaction medium.

Conclusions

This work highlights the powerful influence interfacial potential has on the activities of Brønsted acid catalysts. Although more studies are needed to determine which BAC reactions are most impacted by interfacial potential and the precise mechanistic bases behind their potential dependencies, these findings establish that dramatic changes in rate can be obtained by altering the driving force for interfacial proton transfer steps embedded within an overall non-Faradaic reaction. Altogether, these results indicate that the interfacial potential may play a critical role in heterogeneous BAC reactions, and we posit that other thermochemical reaction classes may also be significantly influenced by this previously underappreciated reaction parameter.

References and Notes

1. S. D. Fried, S. Bagchi, S. G. Boxer, Extreme electric fields power catalysis in the active site of ketosteroid isomerase. *Science*. **346**, 1510–1514 (2014).
2. C. Zheng, Y. Mao, J. Kozuch, A. O. Atsango, Z. Ji, T. E. Markland, S. G. Boxer, A two-directional vibrational probe reveals different electric field orientations in solution and an enzyme active site. *Nature Chemistry*. **14**, 891–897 (2022).
3. N. G. Léonard, R. Dhaoui, T. Chantarojsiri, J. Y. Yang, Electric Fields in Catalysis: From Enzymes to Molecular Catalysts. *ACS Catal*. **11**, 10923–10932 (2021).

4. John O'M. Bockris, Amulya K.N. Reddy, Maria Gamboa-Aldeco, *Modern Electrochemistry 2A: Fundamentals of Electrodics* (Kluwer Academic/Plenum Publishers, New York, New York, ed. 2nd, 2000).
5. J. Wang, F. Xu, H. Jin, Y. Chen, Y. Wang, J. Wang, F. Xu, H. Y. Jin, Y. Q. Chen, Y. Wang, Non-Noble Metal-based Carbon Composites in Hydrogen Evolution Reaction: Fundamentals to Applications. *Advanced Materials*. **29**, 1605838 (2017).
6. S. Díaz-Coello, G. García, M. C. Arévalo, E. Pastor, Precise determination of Tafel slopes by DEMS. Hydrogen evolution on tungsten-based catalysts in alkaline solution. *Int J Hydrogen Energy*. **44**, 12576–12582 (2019).
7. J. X. Wang, F. A. Uribe, T. E. Springer, J. Zhang, R. R. Adzic, Intrinsic kinetic equation for oxygen reduction reaction in acidic media: the double Tafel slope and fuel cell applications. *Faraday Discuss*. **140**, 347–362 (2008).
8. O. Burkan Isgor, J. Ge, J. Ge, O. B. Isgor, Effects of Tafel slope, exchange current density and electrode potential on the corrosion of steel in concrete. *Materials and Corrosion*. **58**, 573–582 (2007).
9. K. ichi Kanno, M. Suzuki, Y. Sato, Tafel slope determination of corrosion reaction by the coulostatic method. *Corros Sci*. **20**, 1059–1066 (1980).
10. J. Zhang, H. B. Tao, M. Kuang, H. Bin Yang, W. Cai, Q. Yan, Q. Mao, B. Liu, Advances in Thermodynamic-Kinetic Model for Analyzing the Oxygen Evolution Reaction. *ACS Catal*. **10**, 8597–8610 (2020).
11. S. Z. Oener, M. J. Foster, S. W. Boettcher, Accelerating water dissociation in bipolar membranes and for electrocatalysis. *Science (1979)*. **369** (2020), doi:10.1126/science.aaz1487.
12. C. G. Vayenas, I. V. Yentekakis, S. I. Bebelis, S. G. Neophytides, In situ controlled promotion of catalyst surfaces via solid electrolytes: the NEMCA effect. *Berichte der Bunsengesellschaft/Physical Chemistry Chemical Physics*. **99**, 1393–1401 (1995).
13. P. Vernoux, L. Lizarraga, M. N. Tsampas, F. M. Sapountzi, A. De Lucas-Consuegra, J. L. Valverde, S. Souentie, C. G. Vayenas, D. Tsiplakides, S. Balomenou, E. A. Baranova, Ionically conducting ceramics as active catalyst supports. *Chem Rev*. **113** (2013), , doi:10.1021/cr4000336.
14. A. A. Khechfe, M. M. Sullivan, D. Zagoraios, A. Katsaounis, C. G. Vayenas, Y. Román-Leshkov, Non-Faradaic Electrochemical Promotion of Brønsted Acid-Catalyzed Dehydration Reactions over Molybdenum Oxide. *ACS Catal*. **12** (2022), doi:10.1021/acscatal.1c04885.
15. V. G. Costas, S. Bebelis, C. Pliangos, S. Brosda, D. Tsiplakides, *Electrochemical Activation of Catalysis: Promotion, Electrochemical Promotion, and Metal-Support Interactions* (Kluwer Academic Publishers, New York, 2001).
16. T. M. Onn, S. R. Gathmann, S. Guo, S. P. S. Solanki, A. Walton, B. J. Page, G. Rojas, M. Neurock, L. C. Grabow, K. A. Mkhoyan, O. A. Abdelrahman, C. D. Frisbie, P. J. Dauenhauer, Platinum Graphene Catalytic Condenser for Millisecond Programmable Metal Surfaces. *J Am Chem Soc*. **144**, 22113–22127 (2022).
17. C. F. Gorin, E. S. Beh, M. W. Kanan, An electric field-induced change in the selectivity of a metal oxide-catalyzed epoxide rearrangement. *J Am Chem Soc*. **134** (2012), doi:10.1021/ja210365j.
18. J. M. Savéant, Electrochemical approach to proton-coupled electron transfers: recent advances. *Energy Environ Sci*. **5**, 7718–7731 (2012).
19. J. M. Mayer, PROTON-COUPLED ELECTRON TRANSFER: A Reaction Chemist's View. *https://doi.org/10.1146/annurev.physchem.55.091602.094446*. **55**, 363–390 (2004).
20. J. N. Schrauben, R. Hayoun, C. N. Valdez, M. Braten, L. Fridley, J. M. Mayer, Titanium and zinc oxide nanoparticles are proton-coupled electron transfer agents. *Science (1979)*. **336**, 1298–1301 (2012).
21. J. F. Keggin, Structure of the Molecule of 12-Phosphotungstic Acid. *Nature 1933 131:3321*. **131**, 908–909 (1933).
22. H. Lund, O. Hammerich, M. Dekker, *Organic Electrochemistry* (Wiley & Sons, New York, 2001).
23. D. T. Sawyer, A. Sobkowiak, J. L. Roberts, *Electrochemistry for Chemists* (Wiley & Sons, New York, 1995).
24. T. S. Wesley, Y. Román-Leshkov, Y. Surendranath, Spontaneous Electric Fields Play a Key Role in Thermochemical Catalysis at Metal−Liquid Interfaces. *Cite This: ACS Cent. Sci*. **7** (2021), doi:10.1021/acscentsci.1c00293.
25. F. Lefebvre, P. Dupont, A. Auroux, Study of the acidity of H3PW12O40 supported on activated carbon by microcalorimetry and methanol dehydration reaction. *Reaction Kinetics & Catalysis Letters*. **55**, 3–9 (1995).
26. C. J. Hastings, R. G. Bergman, K. N. Raymond, Origins of Large Rate Enhancements in the Nazarov Cyclization Catalyzed by Supramolecular Encapsulation. *Chemistry – A European Journal*. **20**, 3966–3973 (2014).
27. W. Schmickler, E. Santos, *Interfacial Electrochemistry* (Springer-Verlag Berlin Heidelberg, Berlin, ed. 2nd, 2010).

28. I. Chorkendorff, J. W. Niemantsverdriet, *Concepts of Modern Catalysis and Kinetics* (WILEY-VCH Verlag GmbH & Co. KGaA, Weinhem, ed. 3rd, 2017).
29. B. C. Gates, J. S. Wisnouskas, H. W. Heath, The dehydration of t-butyl alcohol catalyzed by sulfonic acid resin. *J Catal*. **24**, 320–327 (1972).
30. H. Grisebach, J. B. Moffat, The liquid-phase dehydration of tert.-butyl alcohol on B-P-O catalysts. *J Catal*. **80**, 350–357 (1983).
31. R. E. Warburton, P. Hutchison, M. N. Jackson, M. L. Pegis, Y. Surendranath, S. Hammes-Schiffer, Interfacial Field-Driven Proton-Coupled Electron Transfer at Graphite-Conjugated Organic Acids. *J Am Chem Soc*. **142**, 20855–20864 (2020).
32. M. N. Jackson, M. L. Pegis, Y. Surendranath, Graphite-Conjugated Acids Reveal a Molecular Framework for Proton-Coupled Electron Transfer at Electrode Surfaces. *ACS Cent Sci*. **5**, 831–841 (2019).
33. J. M. Mayer, Bonds over Electrons: Proton Coupled Electron Transfer at Solid-Solution Interfaces. *J Am Chem Soc*. **145**, 7050–7064 (2022).
34. M. F. Delley, E. M. Nichols, J. M. Mayer, Interfacial Acid-Base Equilibria and Electric Fields Concurrently Probed by in Situ Surface-Enhanced Infrared Spectroscopy. *J Am Chem Soc*. **143** (2021), doi:10.1021/jacs.1c05419.
35. M. F. Delley, E. M. Nichols, J. M. Mayer, Electrolyte Cation Effects on Interfacial Acidity and Electric Fields. *Journal of Physical Chemistry C* (2022), doi:10.1021/acs.jpcc.2c01134.
36. L. I. Vergara, M. C. G. Passeggi, J. Ferrón, The role of passivation in titanium oxidation: thin film and temperature effects. *Appl Surf Sci*. **187**, 199–206 (2002).
37. A. E. A. A. Said, M. M. M. Abd El-Wahab, M. M. Abdelhak, The role of Brønsted acid site strength on the catalytic performance of phosphotungstic acid supported on nano γ-alumina catalysts for the dehydration of ethanol to diethyl ether. *Reaction Kinetics, Mechanisms and Catalysis*. **122**, 433–449 (2017).
38. A. Gervasini, A. Auroux, Acidity and basicity of metal oxide surfaces II. Determination by catalytic decomposition of isopropanol. *J Catal*. **131**, 190–198 (1991).
39. R. A. Parker, Static dielectric constant of Rutile (TiO2), 1.6-1060°K. *Physical Review*. **124** (1961), doi:10.1103/PhysRev.124.1719.
40. M. S. Kaba, I. K. Song, D. C. Duncan, C. L. Hill, M. A. Barteau, Molecular Shapes, Orientation, and Packing of Polyoxometalate Arrays Imaged by Scanning Tunneling Microscopy. *Inorg Chem*. **37** (1998), doi:10.1021/ic9705655.
41. B. Fei, H. Lu, W. Chen, J. H. Xin, Ionic peapods from carbon nanotubes and phosphotungstic acid. *Carbon N Y*. **44** (2006), doi:10.1016/j.carbon.2006.02.039.
42. N. T. Jui, J. A. O. Garber, F. G. Finelli, D. W. C. MacMillan, Enantioselective organo-SOMO cycloadditions: A catalytic approach to complex pyrrolidines from olefins and aldehydes. *J Am Chem Soc*. **134** (2012), doi:10.1021/ja305076b.
43. M. Boudart, Two-step catalytic reactions. *AIChE Journal*. **18** (1972), doi:10.1002/aic.690180303.
44. M. Boudart, *Kinetics of Chemical Processes* (Prentice-Hall, ed. 1st, 1968).
45. S. Shukla, D. Stanier, M. S. Saha, J. Stumper, M. Secanell, Analysis of Inkjet Printed PEFC Electrodes with Varying Platinum Loading. *J Electrochem Soc*. **163** (2016), doi:10.1149/2.1111607jes.
46. Z. Y. Liu, J. L. Zhang, P. T. Yu, J. X. Zhang, R. Makharia, K. L. More, E. A. Stach, Transmission Electron Microscopy Observation of Corrosion Behaviors of Platinized Carbon Blacks under Thermal and Electrochemical Conditions. *J Electrochem Soc*. **157** (2010), doi:10.1149/1.3391737.
47. L. K. Jang, R. L. York, L. R. Hile, A note on zero-order reactions in porous catalysts. *Journal of the Chinese Institute of Chemical Engineers*. **34** (2003).
48. W. M. Deen, *Analysis of Transport Phenomena* (1998), vol. 53.
49. D. G. Loffler, L. D. Schmidt, Catalytic activity and selectivity on heterogeneous surfaces with mass transfer. *AIChE Journal*. **21** (1975), doi:10.1002/aic.690210422.
50. R. M. Katona, J. C. Carpenter, A. W. Knight, R. S. Marshall, B. L. Nation, E. J. Schindelholz, R. F. Schaller, R. G. Kelly, Editors' Choice—Natural Convection Boundary Layer Thickness at Elevated Chloride Concentrations and Temperatures and the Effects on a Galvanic Couple. *J Electrochem Soc*. **168** (2021), doi:10.1149/1945-7111/abeb29.
51. M. Eisenberg, C. Tobais, C. Wilke. Ionic Mass Transfer and Concentration Polarization at Rotating Electrodes. *J Electrochem Soc*. **106** (1954)

Acknowledgments:

The authors thank the entirety of the Surendranath and Román labs for their support and feedback throughout this project. We especially thank Prof. Cyrille Costentin, Dr. Neil Razdan, Dr. Hai-Xu Wang, Dr. Jon Kephart, Dr. Ran Zhu, Dr. Jamison Watson, Dr. Mostapha Dakhchoune, Matthew Webber, Kunal Lodaya, Vennala Mannava, Xiao Wang, Melissa Manetsch, Katie Groenhout, and Marcos Farpón for their valuable feedback on the manuscript. We thank Kaylee McCormick and Anna Brenner for their assistance during ICP-MS and GC-MS measurements, respectively. We thank Griffin Drake, Bhavish Dinakar, and Blake Johnson for their assistance in transport phenomenon discussions. We thank Dr. Yong Zhang for assistance during STEM and EDX measurements, Dr. Mohanraja Kumar for assistance during ESI-MS measurements, and Dr. Walt Massefski and Dr. Bruce Adams for assistance during NMR measurements. KSW and TSW acknowledge support from the National Science Foundation Graduate Research Fellowship under Grant No. 174530, and MJH acknowledges support from Schmidt Futures for a postdoctoral fellowship.

Funding:

The studies were supported by the Air Force Office of Scientific Research (AFOSR) under award number FA9550-20-1-0291 and by the U.S. Department of Energy, Office of Basic Energy Sciences, under Award DE- SC0016214.

Author contributions:

Conceptualization: KSW, YRL, YS

Data Curation: KSW

Formal Analysis: KSW, MJH

Funding Acquisition: YRL, YS

Investigation: KSW, MJH, TSW

Methodology: KSW

Project administration: YRL, YS

Resources: YRL, YS

Supervision: YRL, YS

Validation: KSW, MJH

Visualization: KSW

Writing – original draft: KSW, YS

Writing – review & editing: KSW, MJH, TSW, YRL, YS

Competing interests: The authors declare the following competing financial interest(s): KSW, MJH, TSW, YRL, and YS are inventors on patent application #63/513,371, submitted by the Massachusetts Institute of Technology, that covers the use of polarized interfaces to generate Brønsted acid catalysts.

Data and materials availability: All data are available in the main text or the supplementary materials.